Effect of microstructure on the magnetic-field dependence of the local critical current density in $YBa_2Cu_3O_{7-\delta}$ superconductors

L. M. Fisher, V. S. Gorbachev, N. V. Il'in, N. M. Makarov, I. F. Voloshin, and V. A. Yampol'skii

All-Russian Electrotechnical Institute, Krasnokazarmennaya Street, 12, Moscow, 111250, Russia

R. L. Snyder, S. T. Misture, M. A. Rodriguez, D. P. Matheis, V. R. W. Amarakoon, J. G. Fagan, J. A. T. Taylor, and A. M. M. Barus

Institute of Ceramic Superconductivity, New York State College of Ceramics at Alfred University, Alfred, New York 14802

(Received 30 March 1992)

A contactless method for determining the local critical current density $J_c(B)$ and the effective magnetic permeability μ of ceramic superconductors is presented. Using this method we have carried out systematic investigations of the magnetic field and temperature dependence of the local critical current density in $YBa_2Cu_3O_{7-\delta}$ samples with different microstructures. The results show that the character of Josephson junctions in sintered ceramics changes as a function of heat treatment temperature. In spite of the differences in the values of $J_c(B)$ and in the types of Josephson junctions, the dependence of $J_c(B)$ for various kinds of ceramics has a common universal behavior. Using a scaling procedure it is possible to plot all experimental values of $J_c(B)$, obtained for samples prepared by solid-state sintering, on a single curve. At low magnetic fields this universal function is nearly constant with field and at higher fields it varies as $B^{-3/2}$. The universal behavior of $J_c(B)$ breaks down as the field exceeds the first critical magnetic field of the grains, when the function $J_c(B)$ approaches a constant value. The universal behavior is completely defined by the critical current properties of individual Josephson junctions, a set of which forms the network of weak links in ceramics. Flux pinning therefore does not need to be considered when describing the current carrying capabilities of isotropic sintered ceramics which are weak linked. Analogous universal properties of $J_c(B)$ are observed in nontextured samples prepared by melt-processing technology.

I. INTRODUCTION

The discovery of high-T_c superconductors has prompted many research groups to investigate these materials which may be described as a Josephson medium. Many papers have been devoted to the kinetic properties of ceramics and, in particular, to their current carrying capability. High-T_c materials are interesting not only for their potential applications, but also for their unusual electrodynamic properties.

It is clear that the electrodynamic properties of ceramics are defined by the current carrying capability of these materials. The properties of ceramics differ greatly from those of traditional low-temperature superconductors, requiring a different approach to investigations of their physical nature. The difference between high-T_c and conventional materials is greatly exaggerated at low magnetic fields, $H < H_{c1g}$, where H_{c1g} is the first critical magnetic field of the grains. This paper will therefore focus on this magnetic field region.

Earlier,[1,2] a contactless method was developed to determine the local critical current density in ceramic samples using the measured surface impedance. This method was proposed ideologically by Campbell[3] based on Bean's critical state model.[4] The main equation of this model connects the magnetic-field distribution $\mathbf{H}$ inside the superconductor with the local critical current density $\mathbf{J}_c(H)$ as follows:

$$\text{curl } \mathbf{H} = (4\pi/c)\mathbf{J}_c(H) , \tag{1}$$

where c is the speed of light. This formula correctly describes the critical state in homogeneous superconducting materials. Ceramics, however, are inherently heterogeneous materials consisting of a large number of grains connected by a network of weak links. It is commonly accepted that weak links are localized both at the contacts between grains[5] and at twin boundaries within the grains.[6] In describing the current carrying capability it is necessary to take into account intergranular as well as intragranular currents, but the transport J_c is limited by the intergranular currents. J_c is obtained by averaging the intergranular currents over a volume which includes a large number of grains but is small in comparison with the entire specimen volume.

The intragranular currents are accounted for by the parameter μ, which represents the effective magnetic permeability of the ceramic medium when the network of weak links is broken down. According to Dersch and Blatter,[7] μ is defined by the volume fraction of a sample which is penetrated by a magnetic field. μ is equal to

unity in the absence of intragranular currents, for example, when a sample is in the normal state. When intragranular currents exist, some fraction of the grain volume will be screened, decreasing the effective permeability. In addition, intragranular currents at the sample surface will cause a large drop in the induction B at the surface (see Fig. 1).

The critical state model was modified by Dersch and Blatter[7] to apply to such nonuniform materials as high-T_c ceramics. According to their model, the distribution of the magnetic induction $\mathbf{B}$ ($\mathbf{B}$ is the magnetic field averaged over a volume of the sample which contains a large number of grains) is described by the equation

$$\text{curl } \mathbf{B} = (4\pi/c)\mu \mathbf{J}_c(B) \, . \tag{2}$$

The authors of Ref. 7 have pointed out the necessity to account for the strong dependence of the critical current density on B and have noted that the magnetic permeability μ lies near 0.5. The strong dependence of J_c on B results from the sensitivity of Josephson intergranular currents to magnetic fields. The contactless method has shown that the function $J_c(B)$ varies in most cases as $B^{-3/2}$ at intermediate magnetic fields.[2] Approximately the same result was obtained by Peterson and Ekin.[8] As will be shown later, these materials may be modeled as single spherelike Josephson junctions.[9]

At low magnetic fields, as H approaches zero, $J_c(B)$ becomes independent of field strength.[2,8,10,11] This occurs only when the magnetic flux through the junction is less than the magnetic flux quantum Φ_0; under these conditions the maximum undissipative current of the junction remains nearly constant, and J_c remains independent of B.

Although many papers have been devoted to this theme, the majority of the published studies were made by the well-known four-probe method which yields the average critical current density. It is important to note that the four-probe method ignores the self-field of the transport current, while the contactless method proposed in Ref. 2 has no such shortcomings. However, the results obtained in Ref. 2 have some essential limitations. Among these, only the product $\mu J_c(B)$ could be determined instead of the value of J_c which is desired. In addition, the technique applied to cylindrical specimens only. In this paper we consider a modified method which allows measurement of the local critical current density $J_c(B)$ and magnetic permeability μ separately, for either plate-shaped (disc) or cylindrical samples.

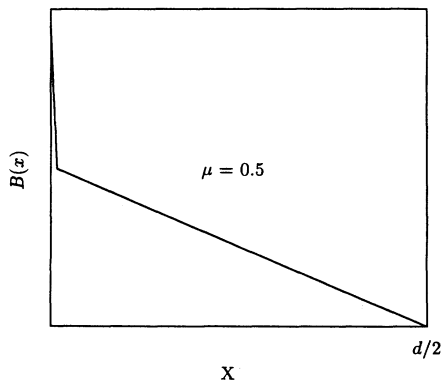

FIG. 1. The distribution of magnetic induction inside a ceramic plate having thickness d and $\mu = 0.5$ (schematically).

Employing this method we have measured the dependence of J_c on B for a variety of ceramic samples prepared by solid-state sintering and melt texturing. In spite of large variations in ceramic microstructure, J_c, and μ, we have observed a universal behavior of $J_c(B)$ for most of the isotropic sintered samples. In the field region $0 \leq B \leq \mu H_{c1g}$ the behavior of $J_c(B)$ for sintered specimens may be described by a single universal function.

II. EXPERIMENTAL PROCEDURE

Several groups of $YBa_2Cu_3O_{7-\delta}$ samples were prepared by different techniques. The main group (samples 1–21) was synthesized from pure Y_2O_3, $BaCO_3$, and CuO powders. The powders were ground in a centrifugal mill, pressed to 92 MPa, and sintered overnight in flowing oxygen. The resulting samples were ground and particles larger than 1 μm were removed. This powder was pressed and heated a second time under identical conditions. The final samples were fabricated by a subsequent grinding and sintering. To obtain specimens with different grain sizes we varied the heat treatment temperature T_h from 870 °C to 960 °C. Plate-shaped samples had a thickness d in the range of 0.5–2 mm. Samples 14–21 were prepared with the addition of 5 mass % Ag.

The second group (samples 22–27) was formed by melt-processing technology. $YBa_2Cu_3O_{7-\delta}$ powders were synthesized by a solid-state reaction of reagent-grade Y_2O_3, $BaCO_3$, and CuO powders. These were ball milled in a plastic bottle with distilled water and zirconia media for 24 h, dried at 90 °C, and granulated using a 40-mesh sieve. The powder was then calcined in air at 925 °C for 18 h, cooled, and reground with a mortar and pestle. The powder was then screened through a 40-mesh sieve, recalcined at 925 °C for 18 h, cooled, and divided into two parts.

The powder was then reground with mortar and pestle and screened through 200-mesh (75 μm) and 325-mesh (45 μm) sieves. A 50% mixture of 200- and 325-mesh powders was pressed at 92 MPa to make 21×3×3 mm bars. The bars were heated to 1050 °C, held for 2.5 h, cooled to 980 °C, held for 100 h, cooled to 550 °C, and held for 36 h, then cooled to room temperature. Heat treatment was carried out in flowing oxygen.

The last group (samples 28–34) was prepared via a sol-gel process employing polyacrylic acid (PAA). Aqueous solutions containing Y, Ba, and Cu were prepared from acetate salts in 1:2:3 stoichiometry. The cation molarity for the solution was in a 0.15 M: 0.30 M: 0.45 M Y:Ba:Cu ratio, respectively. The PAA was mixed into the cation solution so that $\sim$ 1:1 cationic charge to carboxylic ion ratio was attained. The mixture was gelled at 60 °C and dried for 18–24 h at 80 °C. Organic burnout (ashing) was conducted at 600 °C for 5 h. The resultant powder con-

TABLE I. Summary of preparation methods for $YBa_2Cu_3O_{7-\delta}$ samples.

Sample group	Sample number	Powder synthesis method	Heat treatment
1	1–21	Solid state	Sintered in O_2
2	22–27	Solid state	Melt textured in O_2
3	28–34	Sol-gel from acetates	Sintered in O_2

sisted of 100–200-μm agglomerates made up of submicron particles.

Addition of CuO and Ag to a few samples were made by treating the cation solution prior to gelation. The CuO was synthesized by a flow-growth method using an equimolar Na_2CO_3-K_2CO_3 mixture. The Ag was added as a nitrate salt.

The ashed powder was ground to pass a 325-mesh sieve and calcined at 850 °C for 24 h in flowing air. The resulting powder was reground and passed through a 325-mesh sieve before pressing into bars at 20 MPa. The bars were sintered using a heating rate of 100 K/h to 930 °C holding for 6 h, cooling at 100 K/h to 570 °C, holding for a 6-h anneal, then cooling at 200 K/h. This heat treatment was done under flowing O_2. Table I summarizes the sample preparation techniques.

The microstructure and phase content of the samples were investigated using SEM, optical microscopy, and x-ray diffraction using Cu K_α radiation. Grain sizes were determined from SEM micrographs of polished cross sections. Both the length and thickness of the grains were measured directly from the micrographs, and the average grain sizes represent measurements of approximately 100 grains. Other characteristics were measured including geometric density and superconducting transition width determined by resistive and magnetic methods.

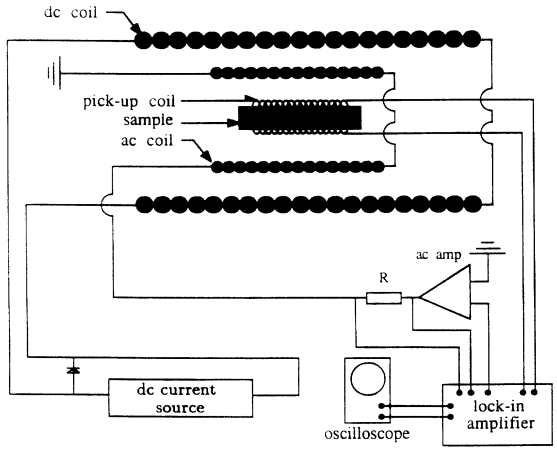

FIG. 2. Schematic of the apparatus used for measuring the surface impedance of a sample. The dc coil method is shown, but an electromagnet could also be used.

To obtain the function $J_c(B)$ the specimen was put into a pick-up coil as indicated in Fig. 2 to measure the surface impedance. The dc magnetic field was applied either using a coil, as shown in Fig. 2, or by means of an electromagnet capable of reaching 2 T. The measurements were carried out at liquid nitrogen temperature, using a frequency $f = \omega/2\pi = 1300$ Hz, and in the magnetic field region of 0–1500 Oe. The magnitude of the ac probe field was less than 1 Oe for measuring sintered ceramic samples. To diminish the influence of the signal connected with losses in grains on the surface impedance, we continuously decreased the amplitude of the ac field to 0.02 Oe at dc fields higher than H_{c1g}. For melt-processed samples, the ac field amplitude was between 1 and 100 Oe. The measurement process was computer controlled, allowing rapid data acquisition and calculations.

III. THEORY OF THE MEASUREMENT METHOD

Consider the penetration of a magnetic field into specimens having two different geometries: a flat plate and a cylinder. These sample geometries are the most convenient experimentally, and some results have been published in Refs. 1 and 2 for cylindrical samples. To conduct the measurement, the sample is placed in a magnetic field having the form

$$\mathcal{H} = \mathbf{H} + \mathbf{h}\cos\omega t \,. \tag{3}$$

The field $\mathcal{H}$ is directed parallel to the plate surface or, for cylindrical samples, along the cylinder axis. Let one of the following conditions be fulfilled:

$$h \ll B^*/\mu \quad \text{or} \quad h \ll H \,. \tag{4}$$

Here B^* is the flux where J_c begins to decrease from its low-field plateau value. Under these circumstances we can neglect the influence of the ac probe field on J_c.

It is well known that the response of a sample to an external field $H(t)$ is described by the surface impedance. The surface impedance $\mathcal{Z} = \mathcal{R} - i\chi$ for a flat plate is determined by the relation

$$\mathcal{Z} = (8\pi/c)E_\omega(x=0)/h, \tag{5}$$

where

$$E_\omega = (\omega/2)\int_0^{2\pi/\omega} E(t)\exp(i\omega t)dt \,. \tag{6}$$

These equations apply when the magnetic field is oriented along the z axis, and the electric field $\mathbf{E}$ is oriented along the y axis. The x axis is perpendicular to the plate, where the points $x = 0$ and $x = d$ correspond to the surfaces of the plate. In the case of a cylinder the surface impedance is defined by Eqs. (5) and (6) where the electric field E has only a ϕ component, which is taken at the surface of the cylinder where $r = R$. The surface resistance $\mathcal{R}$ describes the losses in a specimen while χ is connected with the magnetic field penetration depth. For a full mathematical description we also need the following equation:

$$\text{curl}\ \mathbf{E} = -(1/c)\partial\mathbf{B}/\partial t\ . \tag{7}$$

The boundary conditions for the ac part of the induction, **b**, in both cases may be written in the form

$$\mathbf{b}_{|\text{surface}} = \mu\mathbf{h}\cos\omega t\ . \tag{8}$$

The solution to Eqs. (2) and (5)–(8) permit us to obtain the following relations for the surface impedance for both geometries:

$$\mathcal{Z} = \mu\chi_n F_1(h/h_p) \quad \text{for a disc,} \tag{9}$$
$$\mathcal{Z} = \mu\chi_n F_2(h/h_p) \quad \text{for a cylinder,} \tag{10}$$

where χ_n is the reactance of a sample in a normal state, or

$$\chi_n = 2\pi\omega d/c^2 \quad \text{for a disc,} \tag{11}$$
$$\chi_n = 2\pi\omega R/c^2 \quad \text{for a cylinder .} \tag{12}$$

The functions F_1 and F_2 will be presented later. The penetration field h_p is the ac field at which the ac magnetic induction exceeds zero at every point within the sample volume. The field h_p is defined by the following relations:

$$h_p = (4\pi/c)J_c(\mu H)d/2 \quad \text{for a disc,} \tag{13}$$
$$h_p = (4\pi/c)J_c(\mu H)R \quad \text{for a cylinder .} \tag{14}$$

Notice that the penetration field in (13) and (14) depends on the magnetic field H through the function $J_c(H)$. Since $J_c(H)$ decreases rapidly as H increases, h_p will show similar behavior.

It is clear that Eqs. (9),(13) and (10),(14) determine the connection between J_c, μ, and $\mathcal{Z}(\mu H)$. Equations (10) and (14) were considered in Refs. 1 and 2 for cylindrical samples. Unfortunately, each of the pairs of equations determines only one functional connection between J_c, μ, and $\mathcal{Z}(\mu H)$. We cannot determine the two independent quantities, J_c and μ, having only a single equation.

According to Eq. (2), J_c and μ affect the magnetic-field distribution differently. While μ effects a change of the induction B on a sample surface, the derivative $\partial B/\partial x$ is defined by the product μJ_c. The role of $B(x)$ is illustrated in Fig. 1, for a ceramic disc having homogeneous J_c.

To find an additional equation to determine μ and J_c separately, let us consider the behavior of the function $\mathcal{R}(H)$ in detail. When $h < h_p$ the surface resistance increases with h. However, when $h > h_p$ the induced electric fields penetrating from opposite sides of the plate are compensated. As a result, the surface resistance $\mathcal{R}$ decreases. The surface resistance as a function of H must therefore have a maximum near $h = h_p(H)$. This situation is similar to the phenomenon described in Ref. 12 for the normal skin effect in a metal plate. This simple physical consideration is confirmed by direct calculation. If the magnetic field H is small enough to satisfy $h < h_p$, the functions F_1 and F_2 in Eqs. (9) and (10) can be written in the form

$$F_1(x) = (\tfrac{2}{3}\pi)x[1 - (3\pi i/4)], \tag{15}$$
$$F_2(x) = (\tfrac{4}{3}\pi)x[(1 - 3\pi i/4) - (x/2)(1 - 15\pi i/32)]\ , \tag{16}$$

for $x = h/h_p < 1$. When $h > h_p$, simple formulas exist only for the real parts of F_1 and F_2:

$$\text{Re}F_1(x) = (2/\pi x)(1 - 2/3x)\ , \tag{17}$$
$$\text{Re}F_2(x) = (4/3\pi x)(1 - 1/2x)\ , \tag{18}$$

for $x > 1$. Analyzing these formulas, it is easily seen that the maximum of $F(x)$ occurs at $x = \frac{4}{3}$, or $h = 4h_p(H)/3$ for plates. For cylinders the maximum $F(x)$ occurs at $x = 1$ or $h = h_p(H)$. The maximum values of the surface resistance are described for a plate and a cylinder by

$$\text{Re}\mathcal{Z}_{\max} = R_{\max} = 3(\mu\omega/c^2)d/2 = (3/4\pi)\mu\chi_n, \tag{19}$$
$$\mathcal{R}_{\max} = \tfrac{4}{3}(\mu\omega R)/c^2 = (2/3\pi)\mu\chi_n. \tag{20}$$

Equations (9), (11), (13), (15), (17), and (19) allow μ and J_c to be determined separately for plates. The same treatment applies to Eqs. (10), (12), (14), (16), (18), and (20) for cylinders.

The maximum in $\mathcal{R}$ (H) is reached by increasing the static magnetic field H. Increasing H decreases h_p and, as a result, h_p may become comparable to h at some value of H. Under these conditions $\mathcal{R}(H)$ will be at a maximum, while its position depends on the magnitude of h. Analyzing formulas (13)–(18), it is clear that increasing h leads to a displacement of the maximum position to the region of higher magnetic fields. If we calibrate the plot of $\mathcal{R}(H)$ in units of χ_n we have sufficient information to determine μ and the function J_c (μH).

A list of the necessary equations is included to simplify data analysis. These equations are derived from the above for the critical state parameters of high-T_c samples in terms of the measured surface resistance $\mathcal{R}(H)$.

For plates,

$$\mu = (4\pi/3)\mathcal{R}_{\max}/\chi_n\ , \tag{21}$$
$$J_c(\mu H) = (4ch/9\pi d)\mathcal{R}_{\max}/\mathcal{R}(H) \quad H < H_1\ , \tag{22}$$
$$J_c(\mu H) = (3ch/8\pi d) \times\{1 \pm [1 - \mathcal{R}(H)/\mathcal{R}_{\max}]^{1/2}\} \quad H > H_1\ . \tag{23}$$

Here H_1 is the field H where $h = h_p(H)$. The plus sign in (23) is used in the region $H < H_m$ and the minus sign corresponds to fields $H > H_m$, where H_m is the field at the maximum in $\mathcal{R}(H)$. A simple way to define the value of H_1 is by the relation $\mathcal{R}(H_1) = \frac{8}{9}\mathcal{R}_{\max}$.

For cylinders,

$$\mu = (3\pi/2)\mathcal{R}_{\max}/\chi_n\ , \tag{24}$$

$$J_c(\mu H) = (ch/4\pi R)[\mathcal{R}_{\max}/R(H)] \times\{1 + [1 - \mathcal{R}(H)/\mathcal{R}_{\max}]^{1/2}\} \quad H < H_m\ , \tag{25}$$

$$J_c(\mu H) = (ch/4\pi R) \times\{1 - [1 - \mathcal{R}(H)/\mathcal{R}_{\max}]^{1/2}\} \quad H > H_m\ . \tag{26}$$

Note that in the case of cylinders the field H_1 coincides with H_m.

The proposed method is valid independent of any relation between the ceramic grain size α and London penetration depth λ_L.

IV. RESULTS AND DISCUSSION

A. Physical characteristics

Figure 3 shows the results of the microstructural analyses. Electron micrographs in Figs. 3(a) and 3(b) are polished and etched ceramic samples sintered at 915 and 955 °C, respectively. From these micrographs and the density data listed in Table II, it is obvious that grain growth and densification occur as the heat treatment temperature is increased. The average grain sizes for all samples were measured from similar micrographs. Figures 3(c) and 3(d) show the microstructures of low- and high-J_c melt-processed samples, respectively. The low-J_c sample has large regions ($\sim$ 1 mm) of oriented grains, but these regions are randomly oriented with respect to each other. The high-J_c sample shown in Fig. 3(d) has highly oriented platelike grains. Some of the spherical inclusions in this sample were identified as Y_2BaCuO_5 using energy dispersive spectroscopy.

The x-ray diffraction results are shown in Fig. 4. The pattern labeled (a) is typical of the sintered ceramic materials. All of the ceramics were nearly phase-pure $YBa_2Cu_3O_{7-\delta}$, with small concentrations of Y_2BaCuO_5 present. Figure 4(c) shows the diffraction pattern of the high-J_c melt-processed sample. The (00ℓ) peak intensities are greatly exaggerated, indicating that this sample has highly oriented grains near the surface which was exposed to the x-ray beam. In fact, nearly 100% of the surface grains have their c axes aligned normal to the sample surface. The micrograph of this sample [Fig. 3(d)] shows that this highly oriented grain structure persists completely through the sample cross section. In addition, a small concentration of Y_2BaCuO_5 phase is apparent from the diffraction pattern, confirming the EDS results. The grain alignment is different in the low-J_c melt-processed materials, as shown in Fig. 4(b). The peak intensities are exaggerated in the (00ℓ) and (161) reflections. This result is expected because there are large regions of textured grains which are randomly oriented relative to one another. This sample also contains a small amount of $BaCuO_2$, which is commonly observed in $YBa_2Cu_3O_{7-\delta}$ due to its first peritectic reaction.[13,14] As expected, the overall degree of grain alignment determines the magnitude of J_c.

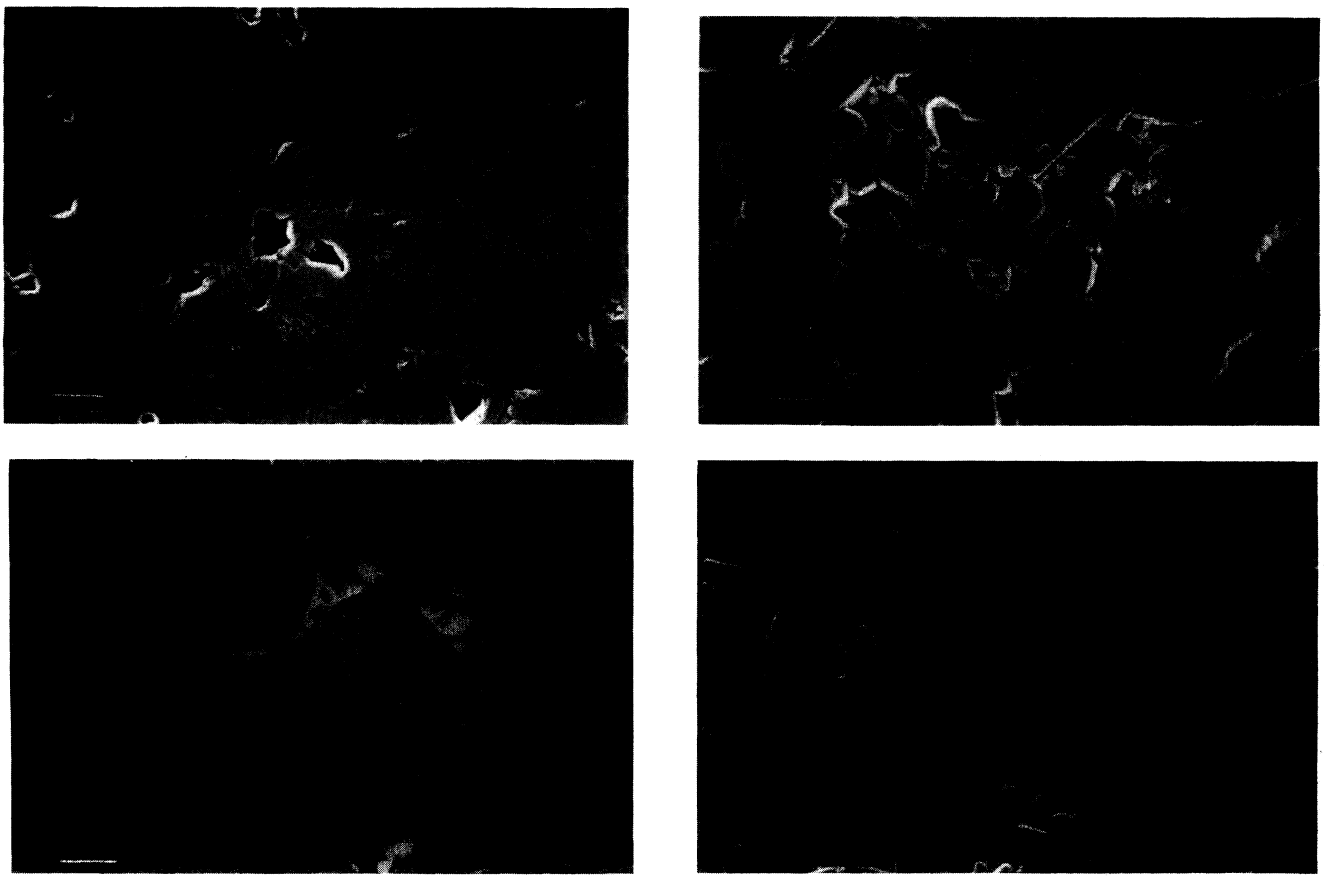

FIG. 3. SEM and optical micrographs of polished and etched samples. (a) Sample 1 with T_h = 915 °C (bar is 10 μm); (b) sample 5, T_h = 955 °C (bar is 10 μm); (c) low-J_c melt processed (bar is 0.25 mm); (d) high-J_c melt processed (bar is 10 μm).

TABLE II. Sample characteristics.

Sample number	T_h (°C)	Density g/cm^3	μ	$J_c(0)$ A/cm^2	B^* Gs
6	920	5.9	0.84	1730	3.8
7	940	6.1	0.42	830	1.9
8	950	6.1	0.2	1170	0.63
9	960	6.1	0.15	545	0.43
10	895	5.0	0.98	315	
23	Melt textured	6.2	0.1	140	0.2
24	Melt textured	6.2	0.04	38	0.12

B. The effective magnetic permeability, μ

Figure 5 shows the typical dependence of the surface resistance $\mathcal{R}/\chi_n$ on applied field H for sample 28, a plate having thickness $d = 1$ mm. The function $\mathcal{R}(H)$ changes slowly at low magnetic field then increases, passes through a maximum, and decreases weakly at higher fields. This behavior is expected from the previous considerations. Using Eq. (21) and the measured maximum value of $\mathcal{R}(H)$, μ is calculated as 0.6. As mentioned earlier, μ is governed by the sample volume where a magnetic field can penetrate. A large fraction of this volume consists of intergranular space and the part of the grains which is occupied by the magnetic field. Naturally, the permeability depends strongly on the ceramic microstructure. The value of μ for samples prepared by the different methods described in Sec. II varies over the range of $0.04 < \mu < 0.99$.

The variation in μ is easily explained on the basis of grain size. The results presented in Fig. 6 clearly show that increasing the heat treatment temperature leads to grain growth. In addition, adding silver to the samples enhanced grain growth at each sintering temperature [compare Figs. 6(a) and 6(b)]. Samples sintered at low temperatures have grain sizes which are about equal to the London penetration depth λ_L; in this case the magnetic field may penetrate the entire sample volume, and μ proves to be about unity. The maximum value of μ was found for samples sintered at temperatures less than 885 °C. In samples with larger grains, intragranular shielding currents expel flux from the grain volume, decreasing the total volume occupied by the field, and decreasing μ. Figure 7 shows the dependence of μ on the grain size for samples prepared by solid-state sintering.

The minimum value of $\mu = 0.04$ is observed for samples prepared by melt growth technology. As will be discussed later, these materials do not have a network of weak links and, in fact, behave like single crystals. The volume of field penetration into such samples is therefore very small, as reflected by the value of μ.

C. Critical current density, $J_c(B)$

Using the surface resistance data and Eqs. (22) and (23) we have obtained the critical current density as a function of magnetic induction. Results for sample 28 (prepared by the sol-gel method) are presented in Fig. 8, which clearly shows a strong dependence of J_c on B. $J_c(B)/J_c(0)$ for samples 6–10, 23, and 24 are shown in Fig. 9 on a log-log scale. This figure shows that $J_c(B)$ defines three different regions of magnetic field. In the

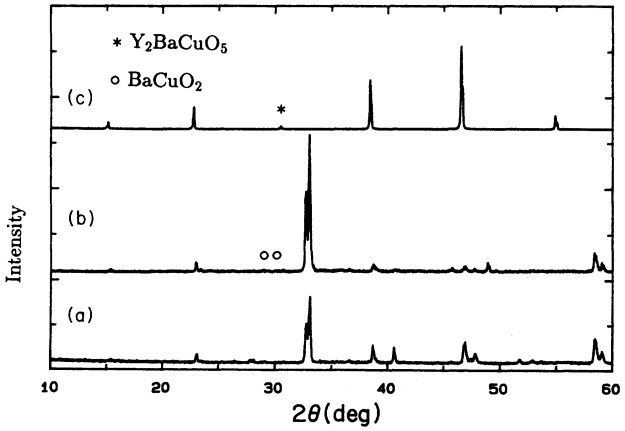

FIG. 4. X-ray diffraction patterns of three types of samples. (a) Typical ceramic, (b) low-J_c melt-processed material, (c) high-J_c melt-processed material.

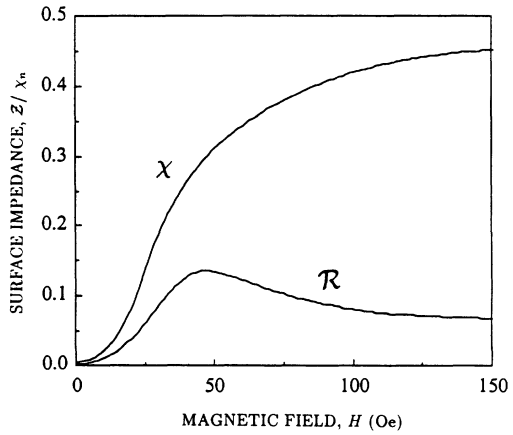

FIG. 5. The dependence of $\mathcal{R}(H)$ for sample 28, prepared by the sol-gel method. Note that the surface resistance is normalized to the normal-state reactance. $T = 77$ K, $d = 1$ mm, $h = 1$ Oe.

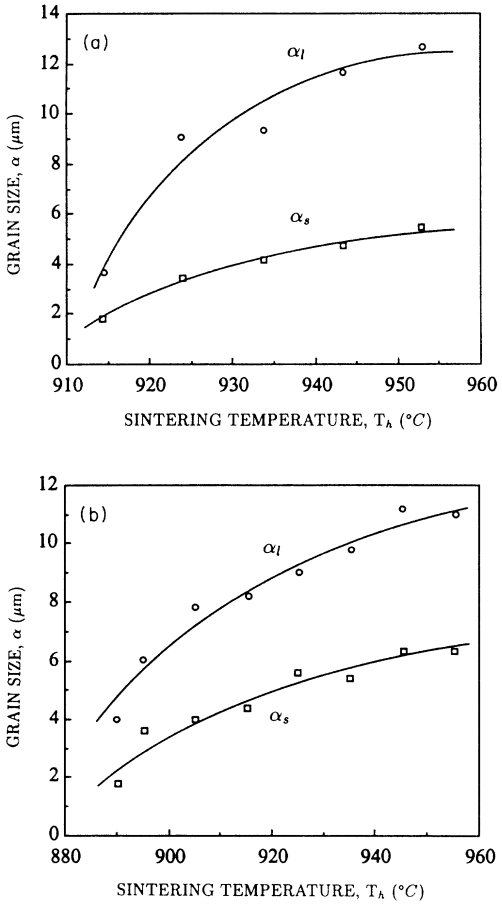

FIG. 6. The grain size dependence on heat treatment temperature in ceramic samples prepared by solid-state sintering. (a) Samples 1–5; (b) samples 14–21 with Ag addition. α_l is the average platelet length, and α_s is the average platelet thickness.

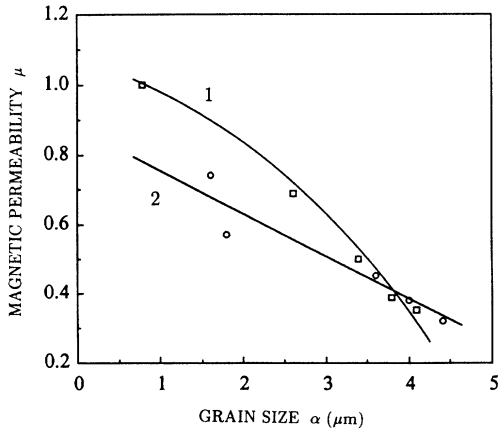

FIG. 7. The dependence of the effective magnetic permeability μ on the grain size in ceramics. Curve 1 corresponds to samples 1–5; curve 2 corresponds to samples 14–21 with Ag addition.

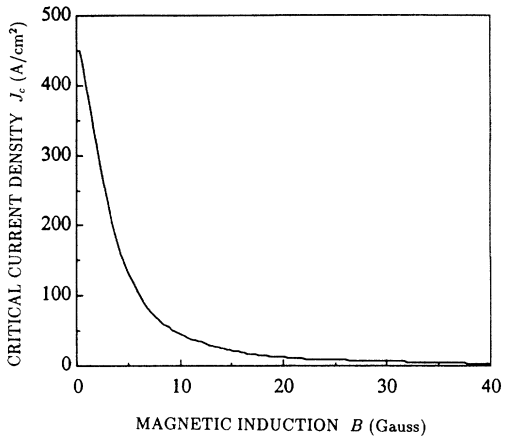

FIG. 8. The dependence of J_c on B for sample 28, prepared by the sol-gel method. $T = 77$ K.

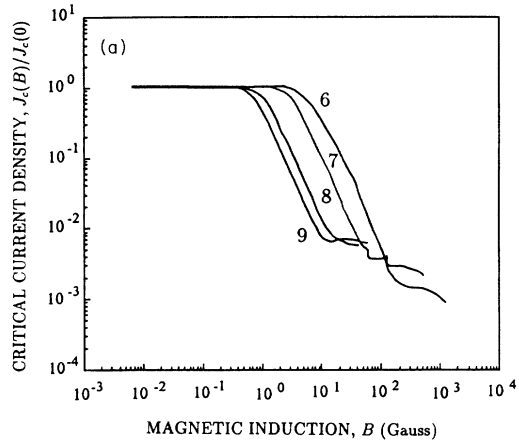

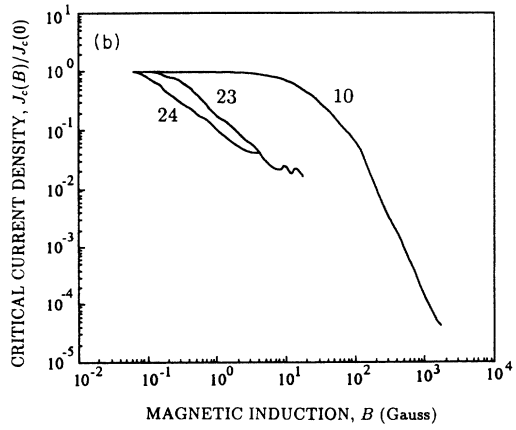

FIG. 9. J_c vs B in log-log scale for different samples at $T = 77$ K. (a) Samples 6–9 as labeled; (b) samples 10, 23, and 24 as labeled. The characteristics of these samples are given in Table II.

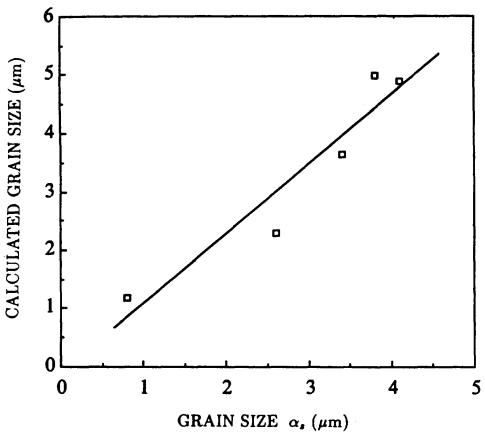

FIG. 10. The correlation between the grain sizes obtained by direct SEM observation (α_s) and the calculated sizes for samples 1–5.

low-field region, the critical current density is approximately constant. This behavior may be understood by considering the properties of a single Josephson junction. The dependence of the critical current I_c on magnetic field for a single plane junction is given by

$$I_c = I_0 |\sin(\pi\Phi/\Phi_0)|/(\pi\Phi/\Phi_0) , \tag{27}$$

where Φ_0 is a magnetic flux quantum and Φ is the magnetic flux through the junction. At low magnetic fields where $\Phi/\Phi_0 \ll 1$ the critical current I_c does not change significantly from its maximum value of I_0. I_c deviates from I_0 only at $\Phi \geq \Phi_0$. We may expect similar behavior in such Josephson media as high-T_c ceramics. For these materials the magnetic flux Φ is related to the grain size α by the estimation $\Phi \cong H\ 2\lambda_L\ \alpha$. A larger grain size results in a larger Φ, and, as shown by Eq. (27), the critical current deviates from its maximum value at lower B. Figure 9(a) shows the sensitivity of $J_c(B)$ on grain size. Evaluations of the junction size obtained from the condition $\Phi \cong \Phi_0$ agree with direct observations as shown in Fig. 10. Although the average critical current density has been measured previously by the four-probe method,[8,10,11] the self-field of the current is large enough to change the low-field results. We believe that this investigation is the first direct observation of $J_c(B)$ at low magnetic field.

As shown in Figs. 8 and 9, the critical current density begins to decrease sharply in the next magnetic field region. As was established in Ref. 2, the dependence of J_c on B is described by a power function $J_c \cong B^{-\alpha}$ in this region. Surprisingly, most of the sintered ceramic samples show this behavior despite their different grain sizes. Figure 9(a) shows that most samples have an exponent near $\alpha = -\frac{3}{2}$. The exceptions are samples with the smallest grain sizes that are comparable to twice the London penetration depth [curve 1 in Fig. 9(b)]. We shall not discuss this result because the theory for the Josephson medium having such a correlation between α and λ_L has not yet been developed.

To confirm that the typical dependence $J_c \propto B^{-3/2}$ is connected with the character of the contacts between ceramic grains, the temperature dependence of J_c was measured. Some results of these measurements are shown in Fig. 11, for 870, 930, and 960 °C. This plot shows that the dependence of J_c on $(1 - T/T_c)$ is described by a power function having an exponent of 2 for the samples with a heat treatment temperature less than 930 °C. For samples with $T_h > 930$ °C, $J_c \cong (1 - T/T_c)^{3/2}$, showing that the contact character changes with heat treatment temperature. It is well known that the first kind of function corresponds to that of an S-N-S contact type, or S-I-S type for superconductors with a short coherence length.[15,16] In the second case the dependence of $J_c(T)$ corresponds to an S-N-I-N-S contact type.[17] Taking into account all of our measurements, we may conclude that the function $J_c(B)$ does not change even when the contact character changes radically.

These results agree with those of Peterson and Ekin,[18] which show that the overall current is defined by the maximum current of a single junction and depends only on the junction geometry.[18] To understand the dependence of J_c on B we can model the ceramic grains as spheres with Josephson contacts between them.[8,18] In the framework of this model the diffraction pattern is described by the formula

$$I_c(H) = 2I_0|J_1(\pi\Phi/\Phi_0)|/(\pi\Phi/\Phi_0) , \tag{28}$$

where J_1 is a Bessel function. After averaging over different grain sizes for the condition $\Phi \gg \Phi_0$, Eq. (28) leads to the dependence $J_c(B) \cong B^{-3/2}$, which is confirmed by our experiments.

The typical dependence $J_c \propto B^{-3/2}$ is invalid for samples prepared by melt processing. Curves 2 and 3 in Fig. 9(b) show that the function $J_c(B)$ varies as B^{-1} for melt-processed samples above the low-field plateau. The difference between ceramic samples prepared by solid-state sintering and melt-processed samples may be attributed to the microstructure. The $J_c \propto B^{-3/2}$ behavior based on Eq. (28) for spherelike Josephson junctions is valid for typical sintered ceramics which have ellipsoidlike

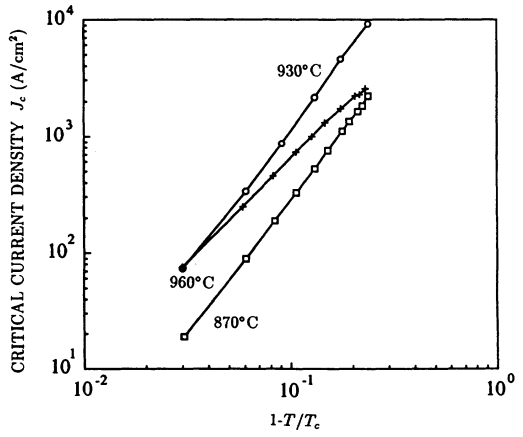

FIG. 11. The temperature dependence of $J_c(0)$ in log-log scale for samples 11, 12, and 13 sintered at the temperatures indicated.

grain geometries. The microstructure of melt-processed materials is completely different, however, so the grain boundary junctions are expected to behave differently. Melt-processed samples have platelike grains whose crystallographic axes are aligned, resulting in planar junctions. The critical current properties of these junctions are therefore described by Eq. (27). After averaging over different grain sizes for the condition $\Phi \gg \Phi_0$, Eq. (27) leads to the dependence $J_c \propto B^{-1}$, which is confirmed by our experiments.

D. Universal dependence of J_c on magnetic induction

1. *Isotropic sintered ceramics*

This type of material, which is formed by solid-state sintering, is exceptionally weak linked and therefore behaves as a Josephson medium. From the above considerations we conclude that the behavior of $J_c(B)$ in sintered samples is analogous to the current carrying properties of a single Josephson junction. The magnitude of $J_c(B)$ is defined by the average parameter I_0, as given in Eq. (28). The magnitude of the variation in $J_c(B)$ for different samples is on the order of B^*, which is defined by the relation $2\alpha\lambda_L B = \Phi_0$. Naturally, the scaling parameter B^* depends on the microstructure of the material, and is different for the various samples. Using B^*, we expect that $J_c(B)$ for any isotropic sintered material can be scaled to a single universal curve.

The universal behavior of several samples is shown in Fig. 12. These results are the same as those given in Fig. 9(a), presented in dimensionless units as $J_c/J_c(0)$ and B/B^*. Note that the solid line in Fig. 12 is the function given in Eq. (28), which describes the magnetic-field dependence of the critical current of a single spherelike Josephson junction. It is clearly seen that all experimental points lie near a single universal curve which intersects points near the local maxima of Eq. (28). Thus we have established the universal behavior of the critical current dependence on magnetic induction for most of the sintered samples in magnetic fields $H < H_{c1g}$. This universal dependence of $J_c(B)$ may be described by the following empirical formula:

$$J_c(B/B^*)/J_c(0) \equiv J_c(y)/J_c(0) = (1+0.3y^3)^{-1/2}, \quad y = B/B^*. \tag{29}$$

Of course, the universal behavior of $J_c(B)$ is not absolute. It occurs in Josephson media only if the grain size is much larger than λ_L and the average properties are homogeneous and isotropic. Note that fine-grained samples do not exhibit universal behavior of $J_c(B)$ because the grain size is comparable with λ_L.

This investigation proves that the critical current density of weak-linked ceramics is fundamentally limited by the individual current carrying properties of a single Josephson junction, a set of which forms a network of weak links in these materials. This means that the widespread conception of pinning is unnecessary for describing the current carrying capability of severely weak-linked ceramics such as those prepared by solid-state sintering.

2. *Melt-processed materials*

A similar type of universal behavior of $J_c(B)$ was found for some of the low-J_c melt-processed samples. The results of the scaling procedure for this type of sample are presented in Fig. 13. The solid curve in Fig. 13 represents the graph of Eq. (27) for a plane Josephson junction. Note that the experimental points define a universal curve which intersects points near the local maxima of

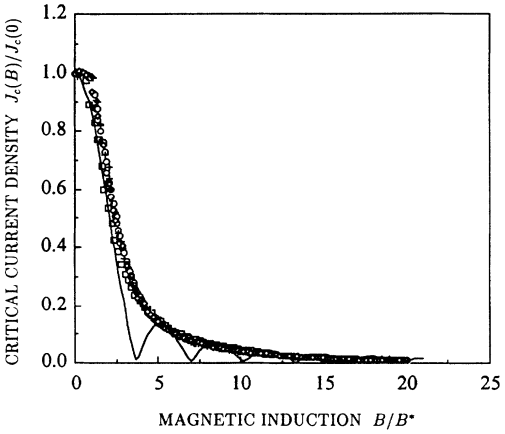

FIG. 12. The universal dependence of J_c vs B in dimensionless units for ceramic samples prepared by solid-state sintering at $T = 77$ K. The solid curve is the graph of Eq. (28), with the data superimposed as follows: (□) sample 6; (○) sample 7; (+) sample 8; (◇) sample 9. The characteristics of samples are given in Table II.

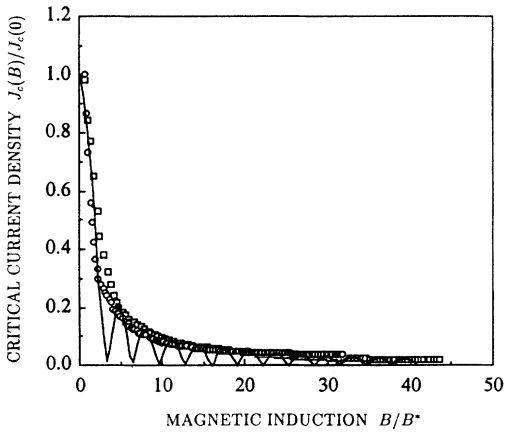

FIG. 13. The universal dependence of J_c vs B in dimensionless units for ceramic samples prepared by melt-processing technology at $T = 77$ K. The solid curve is the graph of Eq. (27), with the data superimposed as follows: (□) sample 23; (○) sample 24. Sample characteristics are given in Table II.

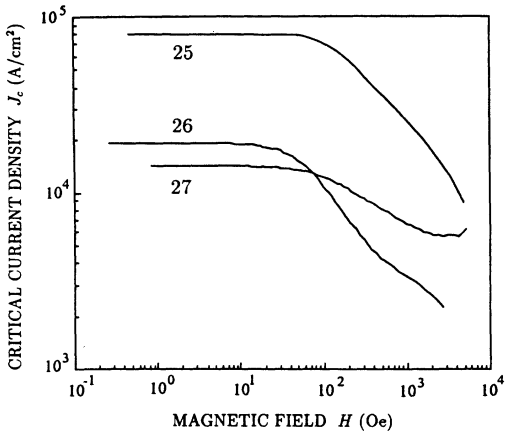

FIG. 14. The dependence J_c vs H for samples 25–27 (as labeled) prepared by the melt-processing technology, $T = 77$ K.

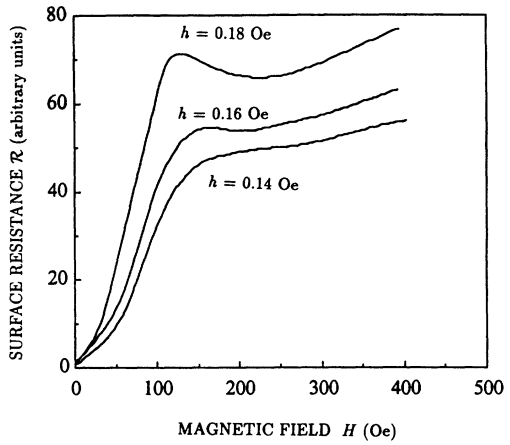

FIG. 15. The dependence of $\mathcal{R}$ on H at several values of the probe field h for sample 12. The amplitude of the probe fields are included in the figure. $T = 77$ K.

Eq. (27). We may approximate our experimental results by the following relation:

$$J_c(y)/J_c(0) = \left(1 + y^3\right)^{-1/3} . \tag{30}$$

High-J_c samples prepared by melt processing have yet another type of $J_c(B)$ dependence. Figure 14 shows that the critical current density J_c is nearly constant over a wide range of magnetic field which is analogous to the $J_c(B)$ behavior of superconducting single crystals. Clearly, the high-J_c melt-processed materials do not contain a network of Josephson weak links, and therefore remain in the Meissner state at fields of $H < H_{c1} \cong 60$ Oe at 77 K. At higher fields Abrikosov vortices begin to penetrate the sample volume and the critical state is established. However, the physical nature of this critical state is different than in sintered ceramics. The critical current density and its dependence on magnetic field are defined by the pinning force affecting Abrikosov vortices. The critical state in these materials is defined by Eq. (1), and the procedure described above for determining J_c vs H remains valid.

E. $J_c(B)$ at high magnetic fields

The universal behavior of $J_c(B)$ in both sintered and low-J_c melt-processed materials occurs only when the magnetic field does not penetrate the grains in the form of Abrikosov vortices. This penetration takes place when an external magnetic field begins to exceed the critical value H_{c1g}, and at larger fields $J_c(B)$ tends to a constant value of J_a.[7] This effect is observed for most of our samples, except the fine-grained ones. Figure 9(a) shows that the high-field plateau starts at different values of B for different samples. This occurs because the local magnetic field around the individual grains is not accurately described by B. Recall that B characterizes the magnetic field inside a sample averaged over a volume containing a large number of grains.[7] In addition, samples having different values of μ will have different effective local fields at grain surfaces. This means that the beginning of the J_c plateaus must be located at induction values $B \cong \mu H_{c1g}$, which qualitatively agrees with our results.

Figure 9(a) shows that the larger grain size samples have larger high-field values of J_c. We cannot give any interpretation of this experimental fact because the behavior of J_c in ceramics is a very complex problem at high magnetic fields. For example, the interaction of Abrikosov and Josephson vortices may cause J_c to increase, resulting in peak effect.[11,19,20] The behavior of $J_c(B)$ in these fields has been examined in a number of papers (for example, Ref. 21), so we will not pursue this subject.

The existence of a high-field plateau on the $J_c(B)$ plot may change the form of the surface resistance dependence on H. As mentioned previously, the position of the maximum in $\mathcal{R}(H)$ is defined by the relation

$$h = \tfrac{4}{3}h_p = (8\pi d/3c)J_c(B) . \tag{31}$$

Since the function $J_c(B)$ exceeds the value J_a everywhere, Eq. (31) cannot be satisfied at $h < 8\pi d J_a/3c$. This means that the maximum in $\mathcal{R}(H)$ does not exist at low h. This effect is demonstrated in Fig. 15 for sample 2. The maximum in $\mathcal{R}(H)$ for this sample is observed at $h > h_{\min} = 0.14$ Oe. The calculated value of h coincides exactly with the experimental value.

V. CONCLUSIONS

The application of an ac probe field is an effective tool in high-T_c materials research. The low-frequency surface impedance has provided a means for the systematic investigation of the critical current properties of high-T_c ceramics. This measurement provides complete information about the electrodynamic parameters of the high-T_c medium. The results are considered valid in application to any ceramic material if the grain size is larger than the London penetration depth. The main conclusions can be summarized as follows.

(1) Using the surface resistance measurement we have

extracted the main parameters characterizing the critical state of superconducting ceramics including the effective magnetic permeability μ and the local critical current density J_c. The study established that the value of μ, which defines the drop of magnetic induction on the surface of a sample, varies over a wide range of 0.04–0.99. The values of μ are governed by the microstructure of the sample and therefore by the preparation technique. We have established the correlation between the ceramic grain size and the value of μ.

(2) The dependence of the critical current density in weak-linked ceramics prepared by solid-state sintering on magnetic induction B may be described by a universal law in the region of magnetic fields where $H < H_{c1g}$. The $J_c(B)$ data for all such samples can be transformed to fit a single curve by a scaling procedure. This universal behavior is observed for all samples which are isotropic and severely weak linked, and can be modeled as a single Josephson junction. At low-magnetic fields the function $J_c(B)$ is independent of field until the magnetic flux quantum is able to penetrate into the junction in the form of Josephson vortex. At higher fields the Josephson vortices penetrate into the junction and suppress the intergranular current, causing J_c to vary as $B^{-3/2}$. This behavior continues up to the first critical magnetic field of the grains, when the magnetic flux penetrates into the medium in the form of both Josephson and Abrikosov vortices. At fields above H_{c1g} the universal behavior of $J_c(B)$ modeled by a single Josephson junction breaks down and the function $J_c(B)$ becomes independent of B. An analogous universal behavior of $J_c(B)$ occurs with low-J_c melt-processed samples.

The universal behavior of $J_c(B)$ leads to an important conclusion about the nature of the critical state in sintered ceramics; J_c is in fact completely defined by the critical current properties of an individual Josephson junction. Flux pinning, therefore, does not have to be considered when describing the current carrying capability of weak-linked ceramics which are most commonly formed by solid-state sintering.

The universal dependence of $J_c(B)$ is invalid for high-J_c samples prepared by melt processing. This result is expected because these samples possess the properties of a single crystal and do not have a network of Josephson weak links.

(3) The temperature dependence of the critical current density was used to determine that the intergranular junction type changes with heat treatment temperature. Samples sintered at temperatures less than 930 °C have S-N-S intergranular junctions, while those sintered above 930 °C have junctions of the S-N-I-N-S type. Nevertheless, the universal magnetic-field dependence of the critical current density remains unchanged because these materials are weak linked.

Many investigations have focused on the electrical and magnetic properties of high-T_c superconductors. The present study includes samples prepared by different methods resulting in three general types of microstructures; isotropic granular, low-J_c melt-processed, and oriented-grain melt-textured materials were investigated. The results show that the $J_c(B)$ behavior of both the isotropic sintered and low-J_c melt-textured samples may be described by two different universal functions at fields below H_{c1g}. This allows one of the most important electrodynamic properties of each of these two types of materials to be simply described using universal relations.

ACKNOWLEDGMENTS

We thank Dr. V.V. Alexandrov for the preparation of several groups of samples and Dr. N. Podlevskikh for useful discussions. This work is supported by Science Council on the Problem of High-T_c Superconductivity (USSR), Project No. 90067 and the New York State Science and Technology Foundation and their Center for Advanced Ceramic Technology.

[1] I.F. Voloshin, N.M. Makarov, L.M. Fisher, and V.A. Yampol'skii, Pis'ma Zh. Eksp. Teor. Fiz. **51**, 225 (1990) [JETP Lett. **51**, 255 (1990)].

[2] L.M. Fisher, N.V. Il'in, O.I. Ljubimov, N.M. Makarov, I.F. Voloshin, and V.A. Yampol'skii, Solid State Commun. **76**, 141 (1990).

[3] A.M. Campbell, J. Phys. C **2**, 1492 (1969).

[4] C.P. Bean, Phys. Rev. Lett. **8**, 250 (1962); Rev. Mod. Phys. **36**, 31 (1964).

[5] J.W. Ekin, J. Appl. Phys. **62**, 4821 (1987).

[6] G. Deutscher, J. Less-Common Met. **150**, 1 (1989).

[7] H. Dersch and G. Blatter, Phys. Rev. B **38**, 11 391 (1988).

[8] R.L. Peterson and J.M. Ekin, Physica C **157**, 325 (1989).

[9] A. Barone and G. Paterno, *Physics and Applications of the Josephson Effect* (Wiley, New York, 1982).

[10] T.K. Dey *et al.*, Solid State Commun. **68**, 635 (1988).

[11] L.M. Fisher, N.V. Il'in, N.A. Podlevskikh, and S.I. Zakharchenko, Solid State Commun. **73**, 687 (1990).

[12] H. Fischer and Y.H. Kao, Solid State Commun. **7**, 276 (1969).

[13] R.L. Snyder, M.A. Rodriguez, B.J. Chen, H.E. Göbel, G. Zorn, and F.B. Seebacher, Adv. X Ray Anal. **35**, 623 (1992).

[14] B.J. Chen, M.A. Rodriguez, S.T. Misture, and R.L. Snyder, in *Superconductivity and its Applications*, edited by Y.H. Kao, P. Coppens, and H.S. Kwok (American Physical Society, New York, 1992), Vol. 4, p. 312.

[15] K.K. Likharev, Pis'ma Zh. Tekh. Fiz. (U.S.S.R.) **2**, 29 (1976) (Russian).

[16] C. Deutscher, IBM J. Res. Dev. **33**, 29 (1989).

[17] B.A. Aminov, N.B. Brandt, Nguyen Min Thuy, Ya.G. Ponomarev, M.V. Sudakova, A.R. Kaul, I.E. Graboi, Yu.D. Tretyakov, J. Wittig, S.P. Kobeleva, L.M. Fisher, and L. Rosta, Physica C **160**, 505 (1989).

[18] R.L. Peterson and J.W. Ekin, Phys. Rev. B **42**, 8014 (1990).

[19] E.G. Zwartz, B.A. Judd, E. Batalla, and L.S. Wright, J. Low Temp. Phys. **74**, 277 (1959).

[20] J.R. Thompson *et al.*, Phys. Rev. B **39**, 6652 (1989).

[21] M.V. Fistul', Pis'ma Zh. Eksp. Teor. Fiz. **49**, 113 (1989) [JETP Lett. **49**, 113 (1989)].

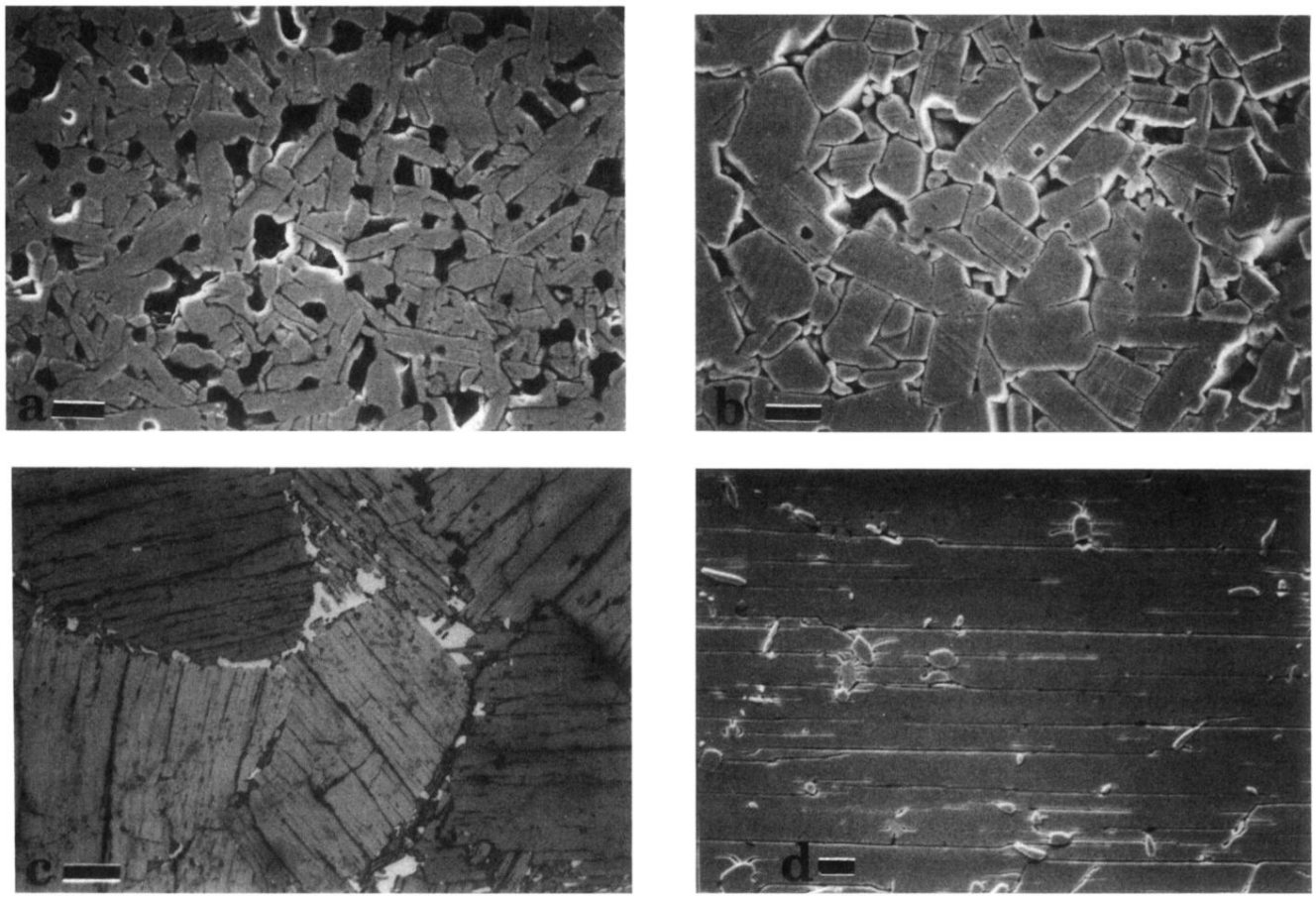

FIG. 3. SEM and optical micrographs of polished and etched samples. (a) Sample 1 with $T_h = 915\,^{\circ}C$ (bar is 10 μm); (b) sample 5, $T_h = 955\,^{\circ}C$ (bar is 10 μm); (c) low-J_c melt processed (bar is 0.25 mm); (d) high-J_c melt processed (bar is 10 μm).